Effect of corrugated minichannel variable width on entropy generation for convective heat transfer of alpha-Alumina-water nanofluid

Effect of corrugated minichannel variable width on entropy generation for convective heat transfer of alpha-Alumina-water nanofluid

N M Muhammad [1,3*], N A C Sidik [1,2], A Saat [1], Y Asako [2], W M A A Japar [2], G H Musa [3] and S N A Yuof [2]

[1] Faculty of Engineering, Universiti Teknologi Malaysia, 81310 Skudai, Johor, Malaysia.
[2] Malaysia-Japan International Institute of Technology. Universiti Teknologi Malaysia, Jalan Sultan Yahya Petra, 54100 Kuala Lumpur, Malaysia.
[3] Faculty of Engineering, Kano University of Science and Technology, Wudil. PMB 3244. Nigeria.

*Corresponding author's email : nuramuaz@gmail.com

Abstract. Energy management and sustainability in thermal systems require maximum utilization of resources with minimal losses. However, it is rarely unattainable due to the ever-increasing need for a high-performance system combined with device size reduction. The numerical study examined convective heat transfer of an alpha-Alumina-water nanofluid in variable-width corrugated minichannel heat sinks. The objective is to study the impact of nanoparticle volume fractions and flow area variation on the entropy generation rate. The determining variables are 0.005 – 0.02 volume fractions, the fluid velocity 3 – 5.5 m/s and heat flux of 85 W/cm^2. The numerical results show an acceptable correlation with the experiment results. The results indicate the thermal entropy production drop with an increase in nanoparticles volume fraction. Contrastingly, the frictional resistance entropy suggests the opposite trend due to the turbulence effect on the fluid viscosity. The induction of Alumina-Water nanofluid with enhanced thermal conductivity declined the entropy generation rate compared to water alone. The increase in width ratio by 16% between the cases translates to at least a 9% increase in thermal entropy production. The outcome of this study can provide designers and operators of thermal systems more insight into entropy management in corrugated heatsinks.

1. Introduction

The recent integration of compact, high-performance electronic devices posed a severe challenge to cooling efficiency due to an overwhelming high heat flux. The dissipation of this heat flux is necessary to reduce the mean time between failure ad increase the lifespan of the devices. The improvement of heat transfer in thermal systems has received much attention recently. The researchers recommended using high thermal conductive liquid-like nanofluids and changes to the flow path [1]. Nevertheless, entropy generation has not been given such preference despite its significance in thermal management and sustainability of systems. Few studies on entropy based on the second law of thermodynamics indicates the varying outcome of thermal and frictional resistance entropy generations [2, 3]. Bejan [4], in his classical work, studied the thermodynamic efficiency of a system. He found entropy as a combined effect of thermal irreversibility and frictional losses. Sohel defined system entropy production as the entropy measure formed by irreversibilities like a chemical reaction, mixing and heat transfer through a

finite temperature gradient [5]. Mir et al. [6] observed an increment in volume fraction of Ag nanoparticles in water enhanced the temperature of the central flow path. For the natural convection, the entropy generation rate was significant at low Gr because of the high-temperature gradient near the elliptical curved minichannel wall. Shahsavar et al. [7] also reported that Fe_3O_4 and CNT concentrations enhance the total entropy generation and convective heat transfer coefficient of the inner and outer walls of the concentric annulus. Mahian and his co-researchers [8] explored numerical analysis of various nanofluids including Cu/water, Al_2O_3/water, SiO_2/water and TiO_2/water on the thermal performance of minichannel flat plate solar collector. They observed minimization of entropy production due to different volume fraction of nanofluids and significant mass flow rate. Ahammed et al. [9] corroborated the findings of Mahian and his colleagues. They observed Re rise from 200 to 1000 at the maximum heat flux of 25 kWm^{-2} leads to the decline of total entropy production by 96% from 0.0361 W/K. Due to recent advantages of computing in machine learning, Bahiraei and Abdi [10] proposed an ANN model to examine the entropy production of TiO_2-water nanofluid in a circular minichannel. The main parameters include Re 500-2000, average concentrations 1% - 4% and particles diameter of 20-80 nm. They found that at a constant heat flux of 10 kW/m^2, the influence of particle migration is substantial on entropy production, especially at high concentration and largest particles diameter. However, the effect is negligible at a low volume fraction of 0.01 and the smallest diameter of 20 nm. They observed that the Bejan number is higher than 0.8 at all concentrations, which implies that heat transfer is responsible for more than 80% of the generated entropy. Other researchers that explored entropy production include [11, 12]. Recently, Huminic and Huminic [13] presented a comprehensive review of works on entropy production using nanofluids in various geometries. They affirmed the advantage of nanofluids in micro/minichannels over the conventional thermal system in achieving effective cooling and reduced entropy generation. Divergent-convergent geometry can recirculate flow and significantly augment heat transfer with moderate pressure loss [14, 15]. Based on the authors' knowledge, the literature has no account of the study on entropy generation in a divergent-convergent minichannel heatsink. The objective is to study the impact of nanoparticle volume fractions and flow area variation on the entropy generation rate using water-based nanofluid in a corrugated minichannel. The outcome of this study can provide designers and operators of thermal systems more insight into entropy management in corrugated heatsinks.

2. Methodology

2.1. Physical models

The study involved divergent-convergent minichannel geometry made of Aluminium substrate. Thus, only a complete and symmetrical unit of the heat sink of the seven parallel minichannels formed the computational domain to minimize the computational cost. For the analysis, two cases C1 and C2, with dimensionless width (w/W) of 0.4 and 0.5, respectively, are considered. Here, w and W represent the minimum and maximum width of the minichannel, as shown in figure 1(a). Thus, the computational domain has 30mm, 3mm, and 2.25 mm as the length, width, and height. Table 1 expressed the geometrical specifications of the cases.

Table 1. Dimensions of the minichannels cases.

Case	w (mm)	W (mm)	Channel height (mm)	Dh (mm)
Case 1	1.0	2.3	1.25	1.42
Case 2	1.0	2.0	1.25	1.36

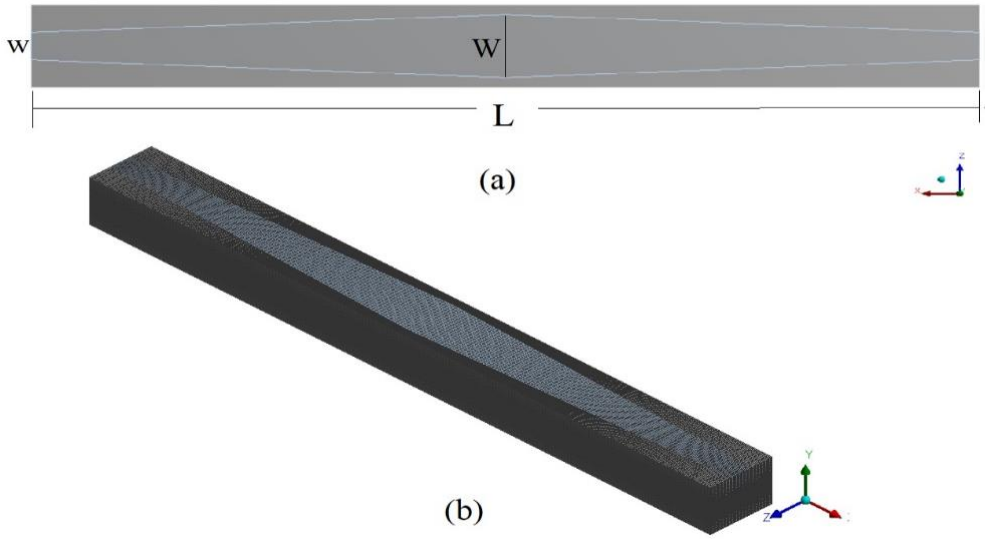

Figure 1. (a) Mesh of the computational domain (b) The top view of the minichannel showing the dimensions.

2.2. Mathematical models

The mathematical modelling made some assumptions to establish the governing equations for the numerical analysis. First, the nanofluid behave as Newtonian fluid flowing in a turbulent continuum through the minichannels. Second, the nanofluid, due to the small volume fraction, dissolve entirely in the water to form a homogenous single-phase mixture. Third, the fluids and solid particles move with the same velocity and exist in thermal equilibrium [16]. Viscous dissipation and radiation are neglected. The thermophysical properties of fluids depend on temperature. The analysis adopted polynomial values of the thermophysical properties used by Bahiraei et al. [17]. Considering the assumptions, the study expressed the Navier-Stokes conservation and energy equations as follows:

Continuity equation:

$$\nabla \cdot \left(\rho \cdot \vec{V}\right) = 0 \tag{1}$$

$$\nabla \cdot \left(\rho \cdot \overrightarrow{V} \cdot \vec{V}\right) = -\nabla P + \nabla(\mu \cdot \nabla \vec{V}) \tag{2}$$

$$\nabla \cdot \left(\rho \cdot \overrightarrow{V} \cdot Cp \cdot T\right) = \nabla \cdot (k \nabla T) \tag{3}$$

Additional equations formulate the turbulent model. The realizable k-ε turbulent model proposed by Shih et al. [18] can effectively simulate the analysis. It has two different equations: the turbulent kinetic energy k and dissipation of this energy ε expressed as follows:

$$\frac{\partial}{\partial t}(\rho k) + \frac{\partial}{\partial x_j}(\rho k v_j) = \frac{\partial}{\partial x_j}\left[\left(\mu + \frac{\mu_t}{\sigma_k}\right)\frac{\partial k}{\partial x_j}\right] + G_k + G_b - \rho\varepsilon - Y_M + S_k \tag{4}$$

$$\frac{\partial}{\partial t}(\rho \varepsilon) + \frac{\partial}{\partial x_j}(\rho \varepsilon v_j) = \frac{\partial}{\partial x_j}\left[\left(\mu + \frac{\mu_t}{\sigma_\varepsilon}\right)\frac{\partial \varepsilon}{\partial x_j}\right] + \rho C_1 S \varepsilon - \rho C_2 \frac{\varepsilon^2}{k + \sqrt{v\varepsilon}} + C_{1\varepsilon}\frac{\varepsilon}{k} C_{3\varepsilon} G_b + S_\varepsilon \tag{5}$$

G_k and G_b represent turbulence kinetic energy generation arising from average velocity gradient and buoyancy, respectively. Y_m is the contribution of the fluctuating dilatation incompressible turbulence to the overall dissipation rate. From equation (5), the values of the model constants are: $C_{1\varepsilon}$, C_2, σ_k and σ_ε are 1.9,1.0 and 1.2, respectively.

The following boundary conditions apply to the current study:

(i) At the inlet of the heatsink minichannel, labelled as "velocity-inlet":
$u = u_{in} = 3 - 5.5\ ms^{-1}$ equivalent to Reynolds number 5000 – 10000. $T = T_{in} = 303K$.

(ii) At the outlet of the minichannel referred to "Pressure outlet": P= 0 Pa.

(iii) A constant heat flux imposed on the bottom wall: $-k_s \frac{\partial T_s}{\partial n} = q = 85\ W/cm^2$

(iv) All other contact surfaces of fluid and substrate experienced no-slip condition and coupled walls:
$u_x = u_y = u_z = 0;\ T_f = T_s;\ -k_s \frac{\partial T_s}{\partial n} = k_f \frac{\partial T_f}{\partial n}$

(v) The two parallel sides of the computational domain are considered as symmetry: $-k_s \frac{\partial T_s}{\partial y} = 0$

(vi) All remaining solid and fluid surfaces are insulated (adiabatic); $\frac{\partial T_s}{\partial x} = 0;\ \frac{\partial T_f}{\partial x} = 0$

2.3. Numerical code and grid sensitivity check

The ANSYS CFD code v17, according to the finite volume method, solved the governing equations in a three-dimensional domain. The COUPLE scheme discretized the equations of pressure and velocity for faster and effective convergence. Convergence set when all the residual diminished below 10^{-6}. The hexahedral mesh mapped the computational domain with a finer grid in the minichannel periphery. The work tested the grid sensitivity to numerical result using three structured mesh (240000, 480000 and 960000) against the finest grid G4 of 1920000 elements. The error of G3 relative to G4 shows 0.48% in terms of the average Nusselt number for water flowing at Re 10000. Hence, the study adopted the third mesh due to its optimal computational time and accuracy, shown in figure 1(b).

2.4. Thermophysical properties of the fluids

In this work, the nanofluid composed of alpha-Alumina nanoparticles dispersed in a distilled water. The volume fractions include 0.005 to 0.02. Table 2 expressed the nanofluids and the base fluid thermophysical properties.

Table 2. Thermophysical properties of base fluid and nanoparticles referenced T = 303K.

Materials	Density (kg/m^3)	Specific heat (J/kg K)	Thermal conductivity (W/mK)	Dynamic Viscosity (kg/ms)
Water (H_2O)	995.1	4182.8	0.603	$799x10^{-6}$
Alumina (α-Al_2O_3)	3970	765	40	-

The nanofluid modelling estimates the effective thermophysical properties appropriately. They include density (ρ), specific heat capacity (C_p), thermal conductivity (k), and viscosity (μ), corresponding to equations (6) – (9) as follows:

$$\rho = (1-\phi)\rho_{bf} + \phi\rho_p \tag{6}$$

$$Cp_{nf} = \left[\phi(\rho Cp)_p + (1-\phi)(\rho Cp)_{bf}\right]{\rho_{nf}}^{-1} \tag{7}$$

$$k_{nf} = \left[1 + 4.4\phi^{0.66}\left(\frac{T}{T_{freez}}\right)^{10}\left(\frac{k_p}{k_{bf}}\right)^{0.03} Pr^{0.66} Re_p^{0.4}\right]k_{bf} \tag{8}$$

where Rep is the particle Reynolds number, its expressed as : $Re_p = \frac{\rho_{bf} k_B T}{3\pi\mu_{bf}^2 l_{bf}}$

The equation is valid for $10 \le dp \le 150$ nm, $0.2 \le \phi \le 9$ % and $294 \le T \le 324$ K.

$$\mu_{eff} = \left[1 - 34.87\left(\frac{d_P}{d_{bf}}\right)^{-0.3}\phi^{1.03}\right]^{-1} \tag{9}$$

where $d_{bf} = 0.1\left(\frac{6M}{N\pi\rho_{fo}}\right)^{1/3}$ where ρ, Cp, k, and ϕ are the density, heat capacity, thermal conductivity, viscosity, and nanoparticle concentration. Whereas the base fluid, the nanoparticle and nanofluid were denoted by subscripts bf, p, and nf, respectively.

2.5. Validation of numerical results

The numerical analysis validates the result with the experimental data for the fully developed turbulent condition of Phillips et al. [19] and Blasius relation [20] for local Nusselt number and average frictional factor, respectively. The analysis used distilled water at Reynolds number 10000. In figure 2(a), the local Nusselt number deviates by about 3%. However, in figure 2(b), the experimental friction factor values vary by around 20% and 4% lower at Re 5000 and 10000. The deviation was primarily attributed to the assumptions proposed during the simulation.

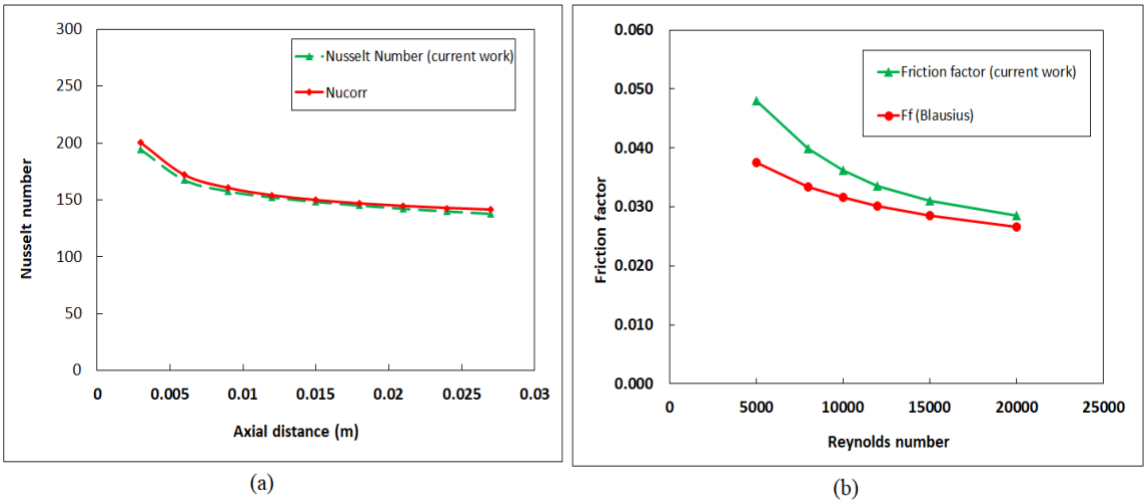

Figure 2. Validation of (a) Local Nusselt number and (b) friction factor.

2.6. Data Processing

In this section, the parameters used to evaluate the thermal performance of the minichannel are presented with appropriate equations as follows:

Equations set (10) evaluates the Reynolds number (Re), average heat transfer coefficient (h), Nusselt number and frictional resistance (f), respectively:

$$Re = \frac{\rho u D_h}{\mu}\ ;\ h_{av} = \frac{q_w}{(T_w - T_f)};\ Nu_{av} = \frac{hD_h}{k};\ f = \frac{2D_h\Delta P}{2L\rho u^2} \tag{10}$$

where ΔP is the pressure differential obtained as the P_{in} - P_{out}. D_h, and L represents the hydraulic diameter, channel length.

The formulation of thermal ($\delta_{gen,th}$) and friction entropies ($\delta_{gen,f}$) and dimensionless Bejan no (Be) are as follows [5]:

$$\delta_{gen,th} = \frac{Q\Pi D_h L}{Nu\ k\ T_b}\ and\ \delta_{gen,f} = \frac{\dot{m}^3 f L}{\rho T_b D_h A_{con}^2} \tag{11}$$

$$Be = \frac{\delta_{gen,th}}{\delta_{gen,th} + \delta_{gen,f}} \tag{12}$$

Q is the sensible heat absorbed by the fluid. A_{con}, ṁ and Π denote the convection area, fluid mass flow rate and the channel perimeter.

3. Results and Discussion

The present paper examined the production of entropy of nanofluids due to thermal and frictional effects in two similar corrugated minichannel heat sinks with a variable maximum width. It involves using a single-phase model for volume concentrations of 0.5 to 2 % with Reynolds number range 5000 – 10000 and constant heat flux of 850 kW/m^2.

3.1. Effect of variable width on thermal entropy production

Figure 3(a) shows that the entropy generation due to thermal irreversibilities decreases with an increase in fluid velocity. The velocity increment dislocates the thermal boundary layer due to the thickening of the hydraulic boundary layer and results in heat transfer enhancement. Therefore, the thermal entropy production is higher in case 1 than in case 2. The reduction of surface area and lower hydraulic diameter in case 2 results in a higher heat transfer coefficient (HTC). It is also clear that an increase in volume fraction of Al_2O_3 in water provides better thermal augmentation due to thermal conductivity enhancement and a rise in mass density. Therefore, the higher the nanofluid volume concentration, the higher the thermal boost and the lower the thermal entropy production. For instance, at 2% Al_2O_3-H_2O nanofluid, the thermal irreversibility reduces by 2.11% and 0.3% compared to water for Case 1 at 3 ms^{-1} and 5.5 ms^{-1}, respectively. Similarly, at the same condition, the reduction is 11.81% and 9.77% for case 2. Comparing the cases, at 2 vol%, the thermal irreversibility is 9.4% and 9.6% higher in case 1 than in case 2 for the corresponding fluid velocities of 3 ms^{-1} and 5.5 ms^{-1}. Hence, the increase in width ratio of 16% translate to at least a 9% increase in thermal entropy production. Therefore, the reduction of surface area can have a significant effect on thermal entropy generation.

3.2. Effect of variable width on Frictional entropy production

Higher fluid velocity depreciates the flow friction resistance and increases hydraulic boundary layer thickness. Therefore, frictional entropy production rises with the increase in the fluid rate for all cases. Also, an increase in Al_2O_3-H_2O volume concentration increases the viscosity significantly. Hence, frictional irreversibility increases with an increase in nanofluid volume fraction. Water indicated the lowest frictional entropy production due to its lower viscosity. However, the viscosity effect in turbulent flow is minor due to insufficient frictional resistance. Hence, it results in the lower contribution of frictional entropy losses. For case 1, the frictional entropy increment between water and 2 vol.% Al_2O_3-H_2O was 18.5% and 18.01% for 3 ms^{-1} and 5.5 ms^{-1}, respectively. For case 2, the frictional entropy production increases by 32.8% and 33.1%, as shown in figure 3 (b). The high values account for reducing hydraulic diameter in case 2, which leads to increased pressure loss and, consequently, a rise in frictional resistance.

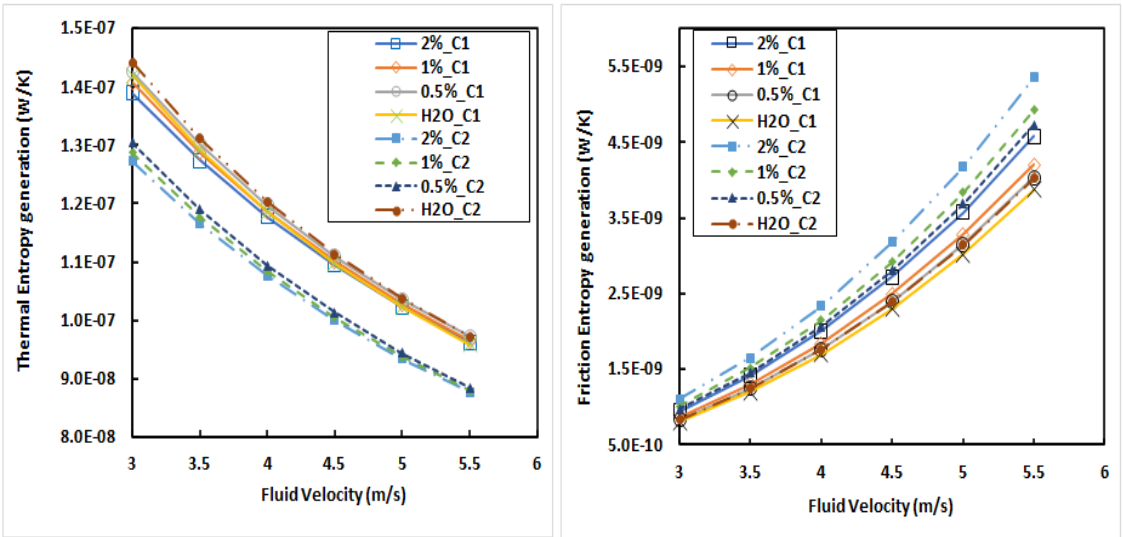

(a) (b)

Figure 3. Entropy generations against fluid velocity for the different cases: (a) Thermal (b) Frictional.

3.3. The comparative effect between the thermal and frictional entropies

The study used Bejan no, expressed as a ratio of thermal entropy to total entropy production, to determine the most influential parameter between the two entropies. The Bejan number decline with the increase in volume concentration and fluid velocity, as shown in figure 4. For all cases, it fell below unity, though it is lower in case 2 for all the volume fractions. The Be values of 0.93 to 0.99 signify that thermal augmentation was responsible for over 90% of the total entropy production. Hence, thermal entropy production was found to be accountable for overall entropy production in the two heatsinks. Therefore, thermal irreversibility should be given much consideration during thermal systems design.

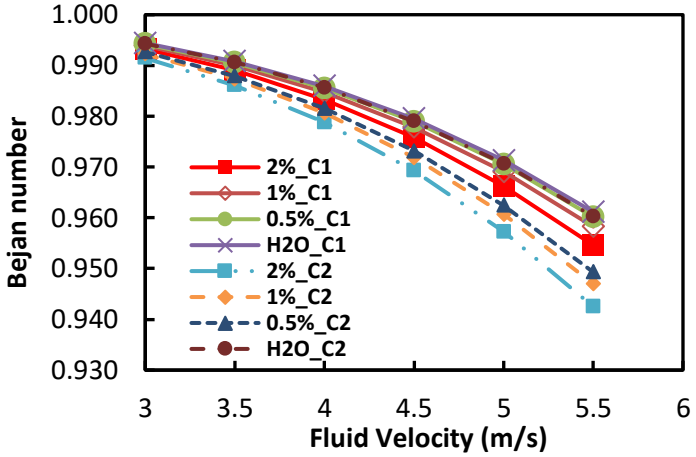

Figure 4. Dimensionless Bejan no as a function of fluid velocity for the cases.

4. Conclusion

The study presented the analysis of irreversibilities in a thermal system due to the application of water and nanofluid in two variable-width minichannel heat sinks. It was observed that entropy generation and dimensionless Bejan number are lower in case 2 due to the lower surface area of the flow domain. The increase in volume fraction of nanofluid results in heat transfer enhancement, especially at lower flow surface area. At 2 vol%, the thermal irreversibility is 9.4% and 9.6%, comparatively higher in case 1 than in case 2 for the corresponding fluid velocities of 3 ms^{-1} and 5.5 ms^{-1}. Since turbulence affects viscosity significantly, the frictional entropy losses are lower with 18.5% and 32.8 % at 5.5 ms^{-1} for case 1 and 2, respectively.

5. References

[1] Liang G and Mudawar I, Review of single-phase and two-phase nanofluid heat transfer in macro-channels and micro-channels, International Journal of Heat and Mass Transfer, 136, 2019. 324-354
[2] Faridi Khouzestani R and Ghafouri A, Numerical study on heat transfer and nanofluid flow in pipes fitted with different dimpled spiral center plate, SN Applied Sciences, 2, 2, 2020. 298
[3] Jiang Y, Zhou X and Wang Y, Effect of nanoparticle shapes on nanofluid mixed forced and thermocapillary convection in minichannel, Int Commun Heat Mass, 118, 2020. 104884
[4] Bejan A and Kestin J, Entropy generation through heat and fluid flow, 1983.

[5] Sohel M R, Saidur R, Khaleduzzaman S S and Ibrahim T A, Cooling performance investigation of electronics cooling system using Al2O3-H2O nanofluid, Int Commun Heat Mass, 65, 2015. 89-93
[6] Mir S, Akbari O A, Toghraie D, Sheikhzadeh G, Marzban A, Mir S and Talebizadehsardari P, A comprehensive study of two-phase flow and heat transfer of water/Ag nanofluid in an elliptical curved minichannel, Chinese Journal of Chemical Engineering, 28, 2, 2020. 383-402
[7] Shahsavar A, Moradi M and Bahiraei M, Heat transfer and entropy generation optimization for flow of a non-Newtonian hybrid nanofluid containing coated CNT/Fe 3 O 4 nanoparticles in a concentric annulus, J Taiwan Inst Chem E, 2018.
[8] Mahian O, Kianifar A, Sahin A Z and Wongwises S, Performance analysis of a minichannel-based solar collector using different nanofluids, Energ Convers Manage, 88, 2014. 129-138
[9] Ahammed N, Asirvatham L G and Wongwises S, Entropy generation analysis of graphene–alumina hybrid nanofluid in multiport minichannel heat exchanger coupled with thermoelectric cooler, International Journal of Heat and Mass Transfer, 103, 2016. 1084-1097
[10] Bahiraei M and Abdi F, Development of a model for entropy generation of water-TiO2 nanofluid flow considering nanoparticle migration within a minichannel, Chemometr Intell Lab, 157, 2016. 16-28
[11] Qiu S, Xie Z, Chen L, Yang A and Zhou J, Entropy generation analysis for convective heat transfer of nanofluids in tree-shaped network flowing channels, Thermal Science and Engineering Progress, 5, 2018. 546-554
[12] Ebrahimi-Moghadam A, Mohseni-Gharyehsafa B and Farzaneh-Gord M, Using artificial neural network and quadratic algorithm for minimizing entropy generation of Al2O3-EG/W nanofluid flow inside parabolic trough solar collector, Renewable Energy, 129, 2018. 473-485
[13] Huminic G and Huminic A, Entropy generation of nanofluid and hybrid nanofluid flow in thermal systems: A review, Journal of Molecular Liquids, 302, 2020. 112533
[14] Muhammad N and Sidik N 2019 Numerical analysis on thermal and hydraulic performance of diverging-converging minichannel heat sink using Al2O3-H2O nanofluid. In: IOP Conference Series: Materials Science and Engineering: IOP Publishing) p 012046
[15] Muhammad N M a, Sidik N A C, Saat A and Abdullahi B, Effect of nanofluids on heat transfer and pressure drop characteristics of diverging-converging minichannel heat sink, CFD Letters, 11, 4, 2019. 105-120
[16] Ying Z, He B, He D, Kuang Y, Ren J and Song B, Comparisons of single-phase and two-phase models for numerical predictions of Al2O3/water nanofluids convective heat transfer, Adv Powder Technol, 31, 7, 2020. 3050-3061
[17] Bahiraei M and Ahmadi A A, Thermohydraulic performance analysis of a spiral heat exchanger operated with water–alumina nanofluid: Effects of geometry and adding nanoparticles, Energ Convers Manage, 170, 2018. 62-72
[18] Shih T-H, Liou W W, Shabbir A, Yang Z and Zhu J, A new k-ϵ eddy viscosity model for high reynolds number turbulent flows, Computers & Fluids, 24, 3, 1995. 227-238
[19] Phillips R J, Microchannel heat sinks, Lincoln Laboratory Journal, 1, 1988. 31-48
[20] Abdolbaqi M K, Mamat R, Sidik N A C, Azmi W H and Selvakumar P, Experimental investigation and development of new correlations for heat transfer enhancement and friction factor of BioGlycol/water based TiO2 nanofluids in flat tubes, International Journal of Heat and Mass Transfer, 2017.

Acknowledgement
The authors thankfully acknowledge the supports funder by the Ministry of Higher Education under FRGS, Registration Proposal No: FRGS/1/2019/STG07/UTM/02/18 & UTM R.K130000.7843.5F273.